Journal of Materials Chemistry C

Low-Temperature, Accelerated Nanoparticle Reshaping for Large-Area, Patterned Plasmonic Nanocomposites

Journal:	*Journal of Materials Chemistry C*
Manuscript ID	TC-ART-02-2018-000780.R3
Article Type:	Paper
Date Submitted by the Author:	16-Jun-2018

Complete List of Authors:	Mahoney, Clare; Air Force Research Laboratory, Materials and Manufacturing Directorate Park, Kyoungweon; Air Force Research Lab, Jawaid, Ali; Air Force Research Laboratory, Materials and Manufacturing Directorate Kowalski, Benjamin; Air Force Research Laboratory; Azimuth Corp Gillman, Andrew; Air Force Research Laboratory, Materials and Manufacturing Directorate Tondiglia, Vincent; Air Force Research Laboratory; Azimuth Corporation, Treml, Ben; Air Force Research Laboratory, Materials and Manufacturing Directorate White, Tim; Air Force Research Laboratory, Vaia, Richard A.; Air Force Research Laboratory, Materials and Manufacturing Directorate

Low-Energy, Nanoparticle Reshaping for Large-Area, Patterned, Plasmonic Nanocomposites

Clare Mahoney[1,2], Kyoungweon Park[1,2], Ali Jawaid[1,2], Benjamin Kowalski[1,3], Andrew Gillman[1,2], Vincent Tondiglia[1,3], Benjamin Treml[1,2], Timothy White[1], Richard A. Vaia[1,*]

[1]Materials and Manufacturing Directorate, Air Force Research Laboratory, Wright-Patterson AFB, Ohio 45433-7702, United States, [2]UES,Inc Dayton Ohio 45432, United States, [3]Azimuth Corporation, Dayton Ohio, 45431

*Email - richard.vaia@us.af.mil

Abstract

Compliant, robust films with pixelated, voxelated or gradient distribution of plasmonic properties are enabling for technologies from colorimetric sensors, filters, and gradient index optical elements to art. Spatially multiplexing different plasmonic effects, however, is challenging. To address this challenge, we demonstrate a post-film fabrication process that enhances gold nanorod (AuNR) reshaping with chemistry. Mild annealing or broadband non-coherent light sources, provide sufficient heating to drive localized redox processes that lead to an isovolumetric reduction of the surface-to-volume ratio of CTAB stabilized AuNRs in polyvinyl alcohol (PVA). Single crystallinity is retained. The reshaping rate in the presence of these redox processes occurs in excess of 100x faster (seconds) than previous reports that utilize increased surface diffusion as temperatures approach the particle melting point (days). Using the process's dependency on reactant concentration, broadband, multi-exposure optical processing preserves particle alignment, enables multi-color patterning, and produces gradients of the longitudinal plasmon resonance of at least 0.01 eV/μm (3 nm/μm).

Keywords:

gold nanorods, plasmonics, nanocomposites, reshaping, redox chemistry, optical patterning

Introduction

Plasmonic materials, and their efficient coupling with light, are driving technologies from ultra-fast computing and compact sensors to medical imaging and therapeutics[1-11]. The optical extinction cross-section and subsequent radiative and non-radiative processes depend on the size, shape, arrangement and composition of the nanostructure, as well as the permittivity and permeability of the environment. [1,12] A subset of emerging technologies, including imaging taggants, colorimetric sensors, and bulk optical components, rely on the response of individual plasmonic units.[13] For such applications, nanoparticles or discrete nanoparticle assemblies are synthesized in solution, surface modified, and deposited on a substrate or dispersed within a film.[1] Notwithstanding the numerous successes of this approach, spatially multiplexing different plasmonic effects within a film is challenging, requiring fabrication of each component followed by site specific assembly.[2,3] Post-fabrication methods that locally reshape a stock plasmonic unit would afford substantial efficiency in constructing such pixelated and voxelated materials. However, available approaches require large energy density, pulsed lasers, lengthy time, or excessive control of reactants to be viable for solid-state patterning at high manufacturing rates or in low temperature matrices, such as polymers, paper and biomaterials.

As a canonical example of an individual plasmonic unit, consider gold nanorods (AuNRs). Their anisotropic shape results in two distinct localized surface plasmon resonances, transverse (T-LSPR) and longitudinal (L-LSPR), where the latter ranges from 550 nm to beyond 1400 nm with aspect ratio (AR) from ca. 1.2 to 10, respectively. This resonance can be further tuned by a gamut

of post-synthesis processes, such as thermal or chemical induced reshaping.[14-21] For thermal reshaping, particle melting or an increased mobility of surface atoms facilitate reshaping, which is driven thermodynamically to a sphere (i.e. minimum surface-to-volume ratio). The onset temperature and rate for reshaping depend on particle size, curvature of local features, ligand stability and rigidity of the surrounding matrix.[14,18,22-26] Heat can be delivered uniformly by a bulk anneal, or locally by non-radiative decay of absorbed photons (plasmonic heating). Clark, El Sayed and others have shown that for plasmonic heating the extent of thermal reshaping depends on duration, pulse width, intensity, and wavelength of the laser irradiation. [27-30] Ultra-fast laser pulses (femto- to nano-second) adiabatically heat the AuNRs since equilibration within the particle of hot electrons to lattice phonon modes occur much faster than thermal diffusion into the matrix. For example, Link, Ziljsta, and others have reported that as the pulse width and energy of the laser increases (i.e. more energy deposited per pulse into the particle), the shape of a AuNR can evolve from entirely unaffected to melted, to fragmented. [22,24,29,31-33] Generally, thermal reshaping of AuNRs via uniform bulk anneals occurs over hours to days. Photo-thermal approaches typically require light sources at ca. 10^{10} W/cm^2. These times, temperatures, and fluences often result in significant damage to the surrounding matrix and/or nanostructure.[34,35]

Chemical reshaping of AuNRs takes place by reduction (overgrowth) or oxidation (etching), and is used extensively in solution synthesis. As with thermal processes, shape evolution can be understand with regard to minimization of interfacial energy. Overgrowth or smoothing of fine features depend on curvature and crystal facet, and occur upon controlled reduction of gold salts,

such as by underpotential deposition or polyol reaction. [20,32,36-38,39] AuNRs etchants include halides and oxygen (e.g. $CN^-/Br^-/Cl^-$ & O_2), H_2O_2, metal salts, or varying acids. Depending on the specific details of the system, the etching rate has been reported to depend on the crystal facet,[40,41] absorbed ligands, and even occurring in the solid state. Coupling of oxidative pathways with regrowth mechanisms is the basis for many approaches to narrow shape distributions, as well as synthesize various monodisperse gold structures through careful manipulation of parameters such as surfactant (in blends and alone), pH, and silver content.[36] Solid-state reshaping though is extreme challenging due to the requisite control of reactant and byproduct concentration.

To construct pixelated and voxelated materials, we demonstrate that solid state reshaping can be enhanced by chemical processes, resulting in accelerated rates and unprecedentedly low optical power densities. Broadband non-coherent light sources, rather than pulsed lasers, are used to provide photo-thermal heating to drive localized redox processes, leading to a reduction in the surface-to-volume ratio of cetyltrimethylammonium bromide (CTAB) stabilized AuNRs in polyvinyl alcohol (PVA) matrix. The nanoparticle volume and its single crystallinity are retained, and complete reshaping with light occurs >100x faster than comparable thermal anneals (10 – 100 sec v. hours to days). Finally, the process's dependency on optical power and reactant concentration provide approaches to spatially control the rate while preserving particle alignment, enabling multi-exposure and multi-color patterning. The utility of this low-cost, rapid

method is demonstrated with fabrication of three dimensional gradient structures and color selective polarization filters with as fine as 3 nm shift in the L-LSPR per micron.

Results and Discussions

Initially, the impact of chemistry on the shape change of CTAB stabilized AuNRs in polyvinyl alcohol (PVA) is established *(Heat-Induced Chemical Reshaping)*. This provides a framework to understand the substantial acceleration in reshaping rate that occurs upon use of broadband light sources *(Photo-Chemical Reshaping).* Finally, these concepts are used to optically fabricate nanocomposites with gradient and patterned plasmonic response *(Optical Patterning)*.

Heat-Induced Chemical Reshaping

As an example of how the optical characteristics of a AuNR-PVA nanocomposite change during heat-induced chemical reshaping, Figure 1 summarizes the evolution of a typical ca. 100 μm film consisting of dispersed CTAB-coated AuNRs (ca. 50 nM) with an aspect ratio (AR = length/diameter, L/d) of 2.8. For reference, at 50 nM the average distance between AuNRs (14 nm x 40 nm) is ~320 nm. With annealing time at 140 ^{o}C (Figure 1d) or with increased temperature at constant annealing time (Figure 1b), the wavelength and intensity of the L-LSPR decreases reflecting a coarsening of the AuNR shape. For example, the L-LSPR blue shifts 180 nm after 60 min at 140 ^{o}C consistent with a reduction in aspect ratio to 1, as shown by TEM (Figure 1c). Note

that this reshaping rate is substantially faster than previous reports of thermal reshaping in solid matrices, where days were required to only partially reduce the AR at a similar temperature.[14,43]

Figure 2 summarizes the dimensional change of the AuNRs during the 140 °C anneal. The AuNRs were extracted by dissolving the PVA films in water, centrifuging to concentrate the extract, and drop casting onto a carbon coated TEM grid. As the AuNR length decreases, the width increases, such that no appreciable change in volume occurs (see SI 1). Additionally, HR-TEM images taken after reshaping indicate that the AuNRs maintain single crystallinity with no additional stacking faults, twinning or defects (Figure 2d and Figure 2e). Retention of crystalline perfection suggests that processes at the surface dominate the reshaping mechanism, rather than alternatives, such as particle fragmentation or routes that would require re-nucleation, such as dissolution. Multiple nucleation events and rapid growth would result in grain boundaries, twin planes and a broadening of the polydispersity.[23] The retention of particle volume and associated volume distribution (Figure 2a, SI1) implies that reshaping is confined to each nanoparticle; that is, it occurs locally and not across the ensemble such as that seen in Oswald ripening.[42] This is in stark contrast to reshaping processes conducted in solution where the concentration of reactants and redox products are considered homogenous throughout the reaction vessel. Rather here the solid-state matrix appears to retard diffusion and spatially localizes precursors to drive isoparticle events.

As noted, the L-LSPR resonance is directly proportional to AR; and estimates of the AR using the empirical relationship for L-LSPR resonance in water (λ_{LSPR} (nm) = (AR)*95 +420) [5] agree with particle dimensions of the extracted AuNRs (see SI2). This further confirms that the spectral observations reflect an isovolumetric transformation (Figure 2a). Therefore, rather than evaluating the rate of shape change by a microscopy-determined aspect ratio, the rate of the reshaping process will be expressed by the shift in the L-LSPR (eV) (see SI3).

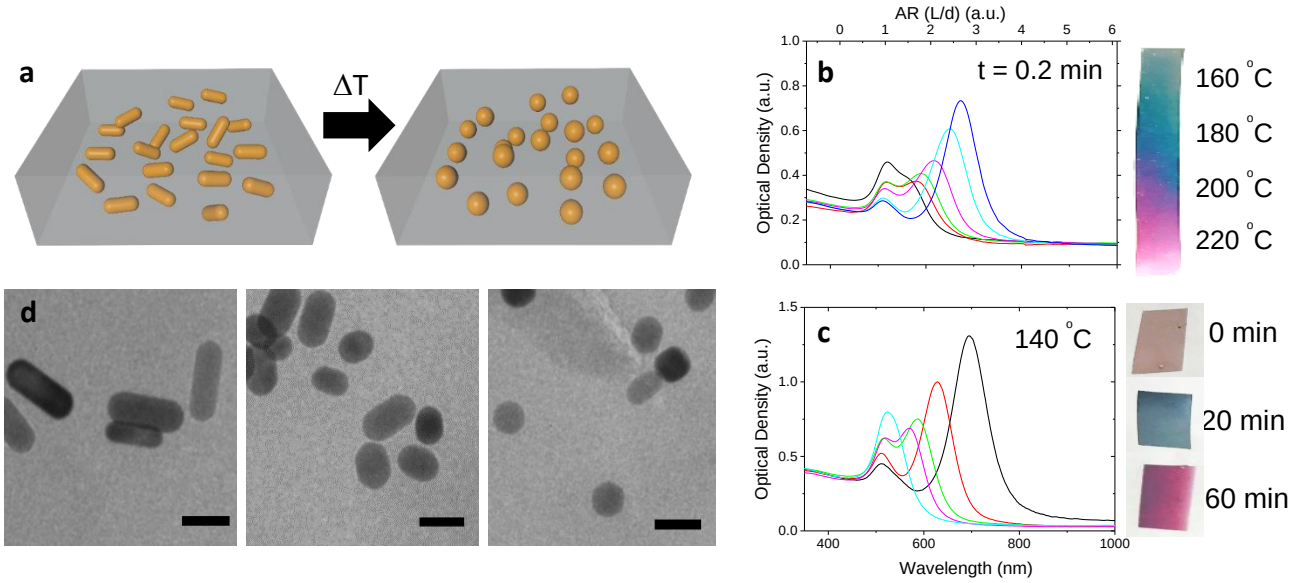

Figure 1. Heat induced chemical reshaping of AuNR in a solid matrix. a) Schematic illustrating the post-fabrication process of restructuring CTAB-stabilized nanorods in poly vinyl alcohol (PVA). The UV-Vis spectra and optical appearance evolve as (b) a function of temperature (160 °C to 220 °C) at 0.2 min, and c) as a function of time (0 min to 60 min) at 140 °C. From left to right, the spectra in b) demonstrate LSPR peak at 160 °C, 170 °C, 180 °C, 190 °C, 200 °C, and 210 °C. From left to right, the spectra in c) show the LSPR peak at 0 min, 15 min, 30 min, 45 min, and 60 min respectively. The initial PVA nanocomposites contains ca. 50 nM of dispersed CTAB-coated AuNRs with an aspect ratio (AR = length/diameter, L/d) of 2.8 the thickness of ~70 μm b) and ~120 μm c). (d) Representative TEM images of the AuNR geometry as L-LSPR wavelength shifts from ca. 700 nm to 630, and to 520 nm (left to right). Scale bar is 25 nm.

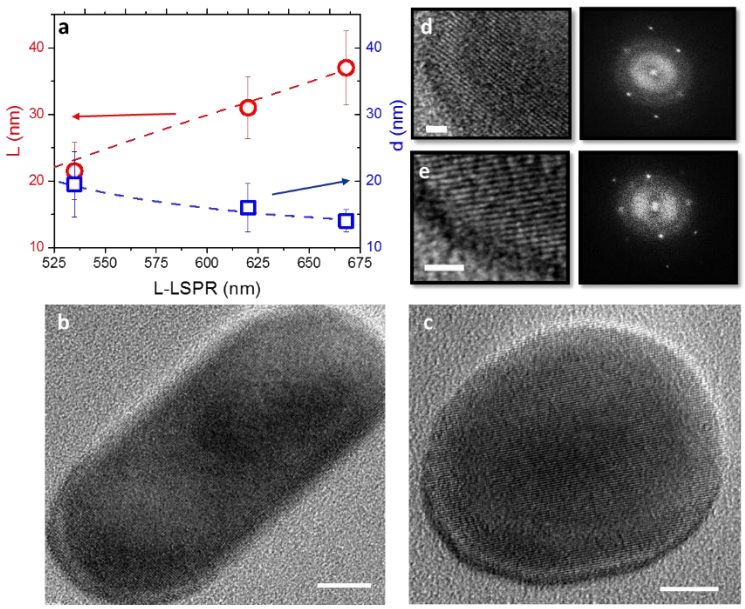

Figure 2. Isovolumetric shape change of the AuNRs during heat-induced chemical reshaping. a) Length (L, red circle) and width (d, blue square) of extracted AuNRs determined from TEM relative to the wavelength of the nanocomposites L-LSPR resonance after 0 min, 15 min, 60 mins at 140 ^{o}C. The initial PVA nanocomposites contained 50 nM CTAB-stabilized AuNRs of AR= L/d = 2.8. Theoretically determined dimensions (dashed lines) under the assumption that individual nanorod volume is conserved agree well with the experimental data as a function of L-LSPR (see SI 1&2). b) and c) High resolution TEM micrographs of reshaped nanoparticles at 15 min and 60 min, respectively (scale bar is 5 nm). d) and e) show lattice fringes (scale bar is 1 nm) and FFT of b) and c) respectively, showing maintenance of crystallinity.

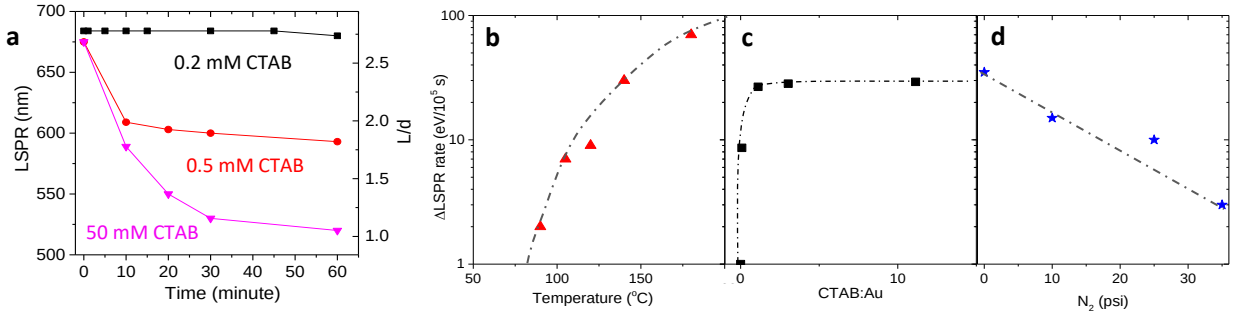

Figure 3. Reshaping rates of AuNR-PVA nanocomposites during bulk thermal anneal. a) The changes in L-LSPR of ca. 100 μm thick PVA nanocomposite films (AuNR L/d = 2.8, ca. 50 nM, aged 3 days) with varying CTAB content as a function of time at ca. T = 140 °C. b) Reshaping rates as a function temperature (in ambient environment and ca. 2CTAB:1Au), c) CTAB:Au ratio (at ca. 140 °C and ambient environment) and d) nitrogen flow pressure (at ca. 140 °C and 2CTAB:1Au ratio, aged 4 days either under identical conditions outside of environment). Dashed lines are provided as a guide to the data trend. (Raw data in SI4).

Figure 3 summarizes the impact of temperature, composition and environment on the rate of change of the L-LSPR of a ca. 100 μm thick PVA nanocomposites containing ca. 50 nM of AuNRs with AR=L/d = 2.8. For example, Figure 3a shows the shift of L-LSPR (nm) as a function of time for nanocomposites with increasing CTAB content. Figure 3 b-d summarizes the initial rate with respect to temperature, CTAB concentration and atmospheric composition, respectively. Reshaping effectively begins at 80 °C for anneals of ~60 min. This is approximately the glass transition temperature of PVA (T_g ~ 80 °C).[43,44] The process accelerates with increased temperature up to approximate 220 °C, Figure 3b. At temperatures above 220 °C, the PVA matrix rapidly degrades (see SI5) and the ability to optically quantify AuNR reshaping is no longer possible. [45,46] It is speculated that using a more thermally stable and reducing matrix would lead to even more accelerated reshaping rates at higher temperatures and/or the onset of additional reshaping mechanisms leading to fragmentation or melting. Note that the reshaping rate reduces by ~10x relative to the aforementioned PVA nanocomposites for AuNRs suspended in a high boiling point solvent (propylene carbonate), without PVA, and with substantially reduced CTAB concentration (L/d = ca. 2.8, ca. 1 nM, [CTAB] < 0.05 mM.) (see SI8). This along with the impact of CTAB concentration and matrix replacement discussed below provides additional confirmation of the importance of chemistry in driving reshaping.

For the nanocomposites examined in Figure 3 (AuNR AR: 2.8 - 6.8), the initial rate exhibits an Arrhenius relationship between 80 °C and 220 °C, yielding an effective activation energy of 0.65 eV (63 kJ/mol) (see SI6). The activation energy for reshaping AuNRs with increasing AR (AR ca. 3-7, See SI 7) was constant (0.65±0.1eV). This contrasts prior work on thermal-triggered reshaping that observed activation energies decreasing with increasing AR (activation energies

ca. 1.5 eV to 0.6 eV for AR from ca. 3 to 6).[47] Finally, reshaping at $T < T_g$ (T~50°C, AuNR-PVA: AR=3.3 and 6.8) was 50x slower than estimated by an Arrhenius extrapolation from $T > T_g$. This substantial retardation indicates that matrix mobility also impacts the reshaping process in the glass. If the matrix mobility did not retard reshaping at T< Tg, then the temperature dependence would be dominated by the activation energy of the reshaping reaction, and the reshaping rate would be similar to that extrapolated from T>Tg.

The reshaping rate also depends on the composition of, and environment around, the nanocomposite. For example, the rate at a given temperature is drastically decreased as the CTAB concentration is reduced. A sharp transition occurs when the molar ratio of CTAB:Au is approximately 2 (Figure 3c, see SI1 for calculation of Au atom concentration). The reshaping rate, and ability to achieve isotropic structures, is approximately independent of CTAB above CTAB:Au ~5-10 as the bromide no longer becomes a limiting reagent in reshaping. Note that decreasing the concentration of CTAB does not affect the interface rigidity surrounding the AuNR since 0.2 mM is still sufficient to form a bilayer of CTAB on all the AuNRs in the nanocomposite (estimated from AuNR concentration and the packing area of CTAB [48]).

Oxygen also impacts reshaping. As the ambient is purged with N_2 at 140 °C, the reshaping rate decreases (Figure 3d). Finally, the duration and nature of storage of AuNRs after their synthesis impacts reshaping. In this work, purified AuNRs (14 x 40 nm; L/d = 2.8, ca. 50 nM) with 25 mM CTAB, aged for 3 days at room temperature and ambient conditions in 20 mL vials (unless

otherwise noted), reshape fast and completely transform to isotropic structures. When an O_2-purged solution of AuNRs (room temperature, aged in Ar atmosphere 4 days, 25 mM CTAB, ca. 50 nM AuNR, AR = 2.8) is used to fabricate a AuNR-PVA film, reshaping at 140 °C under 35 PSI N_2 is completely suppressed. For reference, standard AuNR-PVA film with 50 nM AuNR & 25 mM CTAB at 140 °C in ambient with identical aging conditions outside of environment undergoes reshaping to spheres on the order of minutes. The impact of AuNR storage conditions is consistent with empirically reported changes in AuNR surface reactivity due to continuing crystal facet rearrangement post synthesis.[49] Therefore, to maintain consistent comparison across all nanorod systems used in this study, reported reshaping was conducted after aging (purified and cleaned) AuNR (ca. 50 nM, 14 nm x 40 nm) solutions in 25 mM CTAB for 3 days at room temperature unless otherwise noted.

Overall, the effect of temperature, CTAB, O_2 and AuNR storage conditions points to a chemical surface process driving reshaping. For example, replacement of either CTAB or PVA matrix suppresses chemical reshaping (SI11). The critical stoichiometric ratio between CTAB and the atomic concentration of Au implies that CTAB is a reactant in the process. The role of Br^- from CTAB and O_2 from ambient atmosphere on AuNR oxidation was confirmed with model reactions in aqueous solution by comparing the dissolution of AuNRs stabilized with CTAB (cetyltrimethylammonium bromide) and CTAC (cetyltrimethylammonium chloride) at 90 °C under ambient and inert (Ar) conditions (see SI9). CTAB stabilized AuNRs annealed under ambient oxidized most rapidly, which is expected due to the lowered energy barrier necessary to

oxidize gold when complexed with bromide compared to that of chloride. [50] The color of solution evolved from green to pale pink, clear, and then yellow, indicative of shifting AR until all gold has etched into gold salt. The L-LSPR peak both blue shifted and decreased in intensity until a peak at 262 nm appeared, indicative of $AuBr_2^-$. This behavior corresponds to the AuNRs (AR ~ 2.8) etching into spheres in ca. 15 min, followed by dissolution into $AuBr_2^-$ (salt). In contrast, CTAC coated AuNRs in Ar retained their rod shape after 3 hr heating (see SI9). As for PVA, in situ reduction of gold and silver salts embedded in PVA films through mild thermal annealing have been previously reported[20,21], and confirmed here (see SI10). [43,44,48-52]

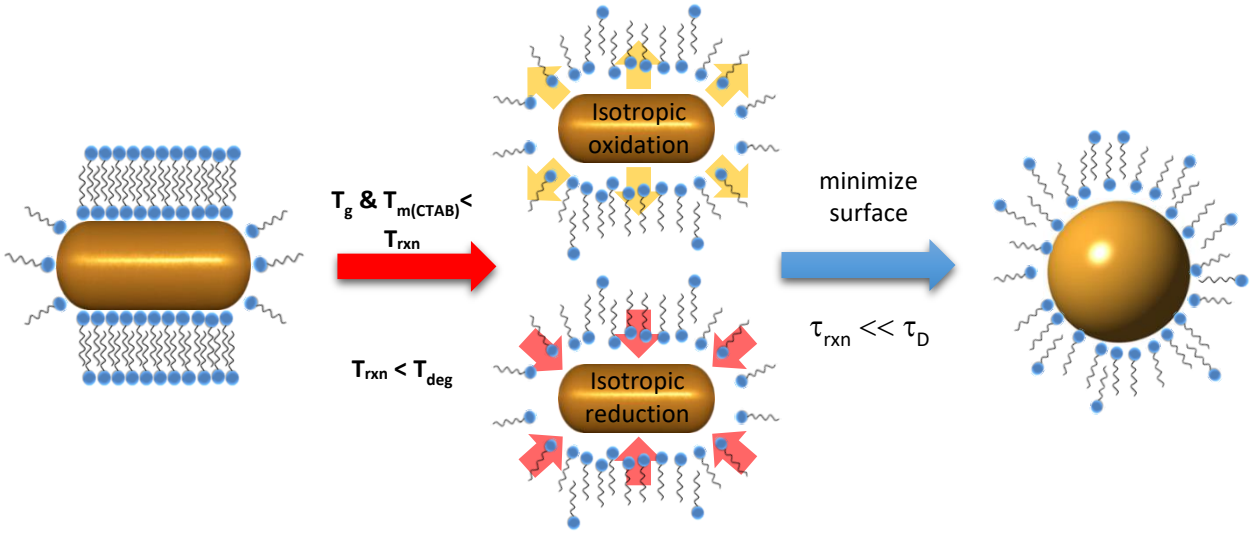

Scheme 1. Heat Induced Chemical Reshaping of AuNR in polymer matrix via redox processes. In the presence of CTAB, O_2 and PVA, oxidation and reduction processes simultaneously occur at the AuNR surface. Mobility near the AuNR surface is created when the reaction temperature (T_{rxn}) is greater than the glass transition temperature (T_g) of the matrix and the melting temperature of the CTAB bilayer ($T_{m(CTAB)}$); but less than the degradation temperature of the matrix (T_{deg}). The gentle heating triggers isotropic oxidation of AuNR to form $AuBr_2^-$. In parallel, $AuBr_2^-$ is reduced through polyol reduction via PVA matrix. These coupled redox processes create an effective mobility of surface Au atoms that respond to thermodynamic driving forces to minimize surface area, leading to an isotropic particle. If the effective transit time of these processes (τ_{rxn}) is substantially less than mass transport between particles (τ_D), the reshaping is isoparticle and isovolumetric.

Scheme 1 summarizes a hypothesized redox process consistent with these observations. The reshaping rate of a particle depends on the flux of atoms moving from regions of high to low curvature. The flux is a product of the concentration of mobile species and their mobility. The mobility and its direction depends on the diffusivity of these species in the environment and the thermodynamic driving force. For reshaping from a rod to a sphere, the driving force is the minimization of surface energy. As noted in the introduction, this is valid for processes dominated by chemistry or those with thermally-driven mobility (i.e. surface melting, etc..). In the absence of chemistry and only considering temperature, the concentration of the mobile species and their diffusivity will depend on the proximity of the temperature to particle melting point, which is size and curvature dependent. Chemistry however can modify both the concentration and diffusivity of mobile species. For example, the concentration of atomic species could also depend on the rate of local reactions, the type of facet, curvature, and surface defects. This reaction rate will also depend on temperature, as noted above. One can also speculate that chemistry could provide alternative pathways for motion by facilitating transport in the near surface region in addition to along the surface. Thus, we hypothesize that a simultaneous and isotropic reduction and oxidation processes at the AuNR surface could enhance the concentration of mobile species, and may even increase their effective diffusivity. The resulting increase in flux accelerates the reduction in surface area and transformation of the spherocylinderical rod to into a thermodynamically stable sphere.

At least four criteria can be envisioned for such a chemically enhanced reshaping arising. First, the local reduction and oxidation processes need to occur at approximately equal rates. If oxidation is much faster than reduction, the AuNR will dissolve into Au salts; and if reduction is much faster than oxidation, the rate of shape will not change. Second, the concentration of reactants for these redox processes must not only be in excess of the total required for dissolution and deposition, but also in balance. Otherwise, one reaction will become limiting and reshaping will not progress towards the thermodynamically stable sphere. Third, the rate of transport of these atomic species must comparable to the rate of these reactions. If the diffusivity is large, long-range Fickian diffusion will deplete the concentration of reactants and products near the AuNR surface. Finally, the local matrix compliance must also be sufficiently low to accommodate local volume redistribution of the particle. All four criteria depend on temperature, as well as the local concentration of reactants and products; where the latter depends on the equilibrium constants of the various chemical reactions.

For the AuNR-PVA nanocomposites, these criteria are likely satisfied by bromide assisted oxidation due to the CTAB ligand; polyol assisted reduction[53,54] due to the PVA matrix; and temperatures greater than the matrix T_g and melting point of the ligand bilayer, $T_{m(CTAB).}$ For reduction, the PVA matrix serves as a weak reductant (polyol), continually transforming $AuBr_2^-$ to Au (0). For oxidation, it is hypothesized that the bromide ion associated with CTAB is partially oxidized into elemental bromine in the presence of atmospheric oxygen at the elevated temperature. No mechanistic steps on the progression of oxidation however have been

hypothesized, although it is likely that that Br^- complexes with Au(II) and Au(0) to stabilize intermediates.[21,41] This proposed mechanism is consistent with the threshold CTAB:Au molar ratio of 2 (Fig. 3b), and oxidative dissolution of AuNRs in the presence of CTAB and O_2 in solution at 90 °C. Additionally, the activation energy of the process is unchanged with CTAB:AuNR <2, only the absolute rate is reduced (see SI6). Note that prior reports emphasize that AuNR oxidation preferentially occurs at the end of the rods, due to a more robust CTAB bilayer on the side that inhibits etching.[41,55] However for the temperatures of reshaping, the structure of the CTAB bilayer is destabilized (T_m ~ 90°C), facilitating isotropic etching. [56,57]

Finally, the isotropic character of the redox processes implies that the initial rate of reshaping (i.e. rate of change in aspect ratio) should be greater for rods with larger aspect ratios, since there is more surface area. This can be expressed in the large AR limit by considering the volume of intersection between a sphere of radius, r, and a cylinder of radius, R, with length, L = 2αR, whose centroids are coincident and where α is the aspect ratio, AR.[58] In the case of isovolumetric reshaping, the particle volume, V, is constant and r > R. The fractional volume that has to be transported for complete transformation from a rod to a sphere is then:

$$\frac{\delta V}{V} = \left(1 - \left({}^{3}/_{2}\,\alpha\right)^{{}^{-2}/_{3}}\right)^{{}^{3}/_{2}} \quad (1)$$

The initial rate of change of the aspect ratio then depends on α and V as:

$$\frac{d}{dt}(\alpha) \sim A\,V^{-1}\left[\frac{\left(\frac{3}{2}\alpha\right)^{{}^{5}/_{3}}}{\left(1-\left(\frac{3}{2}\alpha\right)^{{}^{-2}/_{3}}\right)}\right] \quad (2)$$

where the local volume transfer rate is assumed constant, $d(\delta V)/dt = A$. Note that that this expression does not approach zero as $\alpha \to 1$. This is due to the assumption that the initial structure is a truncated cylindar of radius R, which does not smoothly transform to a sphere nor have the same volume of a sphere when r = R. The scaling however between the initial rate of AR change, the AR, and volume are consistent with numerical models. The model and analytical derivation is detailed in SI12.

Overall, the experimental trends qualitatively agree with these models. As the particle volume increases, the initial reshaping rate, as expressed as the rate of change in L-LSPR, is seen to decrease. Also, as the AR increases, the initial reshaping rate is observed to increase. For example, the ratio of reshaping rate at 140 ^{o}C of two identical PVA nanocomposites containing 50 nM AuNRs with similar volume (~ 8000 nm^3) but different AR (AR = 3.3 and 6.8) was ~2.7. The model predicates a ratio of 2.1. Furthermore the activation energy of the process does not depend on AR (see SI6). This provides further corroboration that the local surface chemistry underlying the process summarized in Scheme 1 occurs uniformly around the particle.

Photo-Chemical Reshaping

The proposed redox processes that drive solid state reshaping should also be triggered photo-thermally due to the non-radiative decay of AuNR plasmon resonances.[30,59,60] Figure 4a summarizes the photo-thermal response of a typical AuNR-PVA film (ca. 100 μm, 50 nM, AR =

2.8) supported on a glass substrate exposed to broadband light from a Xenon Arc Lamp (total measured power density across the wavelength of 190-2500nm ~ ca. 1-13 W/cm^2). Optical heating is very rapid, for example a steady state temperature of 120 ^{o}C can be reached in less than 20 seconds.

Using energy conservation; the optical energy absorbed can be completely accounted for by the known physical parameters of the system. The film's temperature can be understood as (see SI12): [61]

$$m\, C_p\, {d\Delta T}/{dt} = Q_{in} - Q_{out} \quad (3)$$

$$Q_{out} = -hA(T - T_\infty) \quad (4)$$

$$Q_{in} = \eta_{NR}\, I_{abs} \quad (5)$$

where the rate of change in temperature of the sample ($d\Delta T/dt$) is related to the difference in the rate of energy absorbed (Q_{in}) and dissipated (Q_{out}) by the sample of mass, m and specific heat capacity, C_p. For the temperature range examined, the rate of heat loss to the environment, Q_{out}, will be dominated by convection and conduction; and according to Newton's Law of Cooling proportional to the linear thermal driving force (T-T_∞) by the product of the heat transfer coefficient, h, and sample area, A. The rate the system heats, Q_{in}, will scale with the fraction of optical energy absorbed that is emitted in the form of heat, η_{NR}. For these AuNRs, it is reasonable to assume $\eta_{NR} \approx 0.8$. [5,35] The optical energy absorbed, I_{abs}, is related to the absorbance of the sample, A_λ, via Beer-Lambert's law as $I_{abs} = I_0(1 - 10^{-A_\lambda})$, where , $A_\lambda = \varepsilon\, \ell\, c$, ε is molar

absorptivity, ℓ is path length, c is AuNR concentration, and I_0 is incident intensity (see SI13). The energy absorbed was both calculated from the product of the film absorbance and incident light intensity spectrum as well as experimentally measured with a power meter (Figure 4b). Note that PVA is optically transparent across the wavelength range and contributes negligibly to heating from irradiating light (experimentally demonstrated in SI 14). At steady state, $Q_{in} = Q_{out}$ and thus the slope of Fig 4b quantifies the proportionality hA for a given sample geometry across a large range of incident intensities and concentration of AuNRs in PVA. When the intensity is removed, $Q_{in} = 0$ and the temperature decay will be defined by mC_p/hA – all of which are known. mC_p determined from the thermal observations in Figure 4 are in good agreement with that known for PVA film on glass (see SI13). The dashed line in Fig 4b captures the systems behavior for a broad range of nanocomposites with different AuNR concentration and aspect ratio; and the dashed line in Figure 4a shows the quantitative agreement between sample cooling and derived material parameters. This confirms the utility of this simple thermal model to understand and control sample temperature for a given nanocomposite, illumination source and geometry.

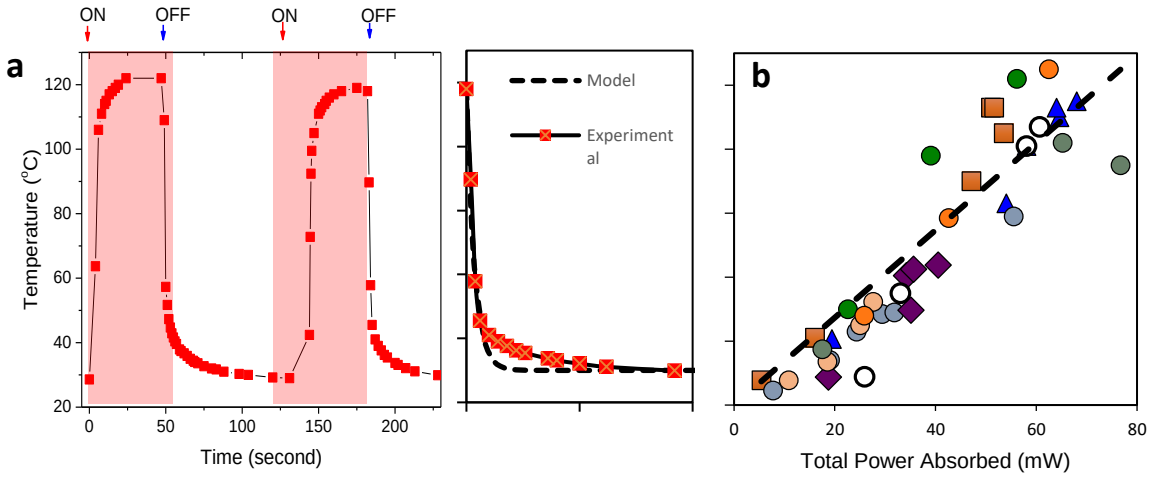

Figure 4. Photo-thermal heating of AuNR-PVA nanocomposite films using broadband light. a) The change of bulk temperature of a AuNR-PVA film (100 μm, 50 nM, AR = 2.8) during the cycling of light-on and light-off. The power density of broadband light was ca. 10 W/cm^2 and the spot size was ca. 1.5 mm. The bulk temperature was determined by FLIR thermal camera. Cooling agrees with simple bulk thermal diffusion model (Eqn. 3-4). b) The net temperature increase seen in bulk films (supported on a glass substrate) as a function of power absorbed. The steady state temperature scales linearly with the overall power absorbed, regardless of CTAB content, AuNR dimension and AuNR concentration. Each symbol and color indicates a different AuNR-PVA nanocomposite with values ranging from 0-50 mM CTAB, 10-257 nM AuNR, and AR from 1-6 (see SI15 for specific features of each film). The power density of broadband light was varied from ca. 1 to 13 W/cm^2.

For AuNR concentrations (1-250 nM) and continuous irradiation conditions (1-13 W/cm^2) used herein, each AuNR is radiating approximately picowatts (pW) of heat into the surrounding matrix. The local steady-state temperature profile around an absorbing AuNR can then be estimated using the thermal diffusion equation, assuming each AuNR acts as an isolated heat source (see SI13). This is reasonable since (a) the continuous illumination is orders of magnitude longer than thermal equilibration of the plasmon excitation to the nanoparticle lattice and local environment (~ nanoseconds),[63] and (b) the particle-particle distance (~320 nm) is substantially greater than effective particle size (effective radius ~ 10-15 nm). All the physical parameters to determine the temperature profile from the AuNR to the bulk are then known except for the interface

conductance. Losego et. al reported that the interface conductance of a ligand-gold surface ranged from ca. 34 MW/m^{2}K to 65 MW/m^{2}K as the strength of the ligand binding increased (van der Waals to covalent). [62] Using this as an estimate for interface conductance, the thermal diffusion equation yields a temperature increase at the AuNR of ca. 0.0007K - 0.0015 K relative to the bulk. Using the activation energy from our oven experiments, we estimate the difference between the bulk temperature revealed by the IR camera and the AuNR must be at least 100-200K to account for the observed increase in reshaping rate (discussed below). For this, the thermal boundary conductance would have to be ca. 10^5 times lower. This is well below any established value of thermal boundary conductance reported in literature, which range from ca. MW/m^{2}K to GW/m^{2}K. It is useful to note that experiments have demonstrated non-equilibrium heat localization around gold nanostructures in fluids, for example the generation of steam in water. [61-65] However, the irradiation power density ca. 10^4 W/cm^2 in these experiments are 3-orders of magnitude greater than in ours (power density ca. 10 W/cm^2). Thus, these estimates imply that for the conditions used herein, photo-thermal heating via plasmon decay should result in a uniform sample temperature even at the nanoscale.

Controlled reshaping is demonstrate in Figure 5. Figure 5a shows the evolution of the absorbance spectra of a typical AuNR-PVA film (AR = 2.8, 100 nM AuNR, 100 μm thick) when irradiated with broadband light at ca. 10 W/cm^2, corresponding to a film temperature of ca. 140 ^{o}C. The L-LSPR peak shifts from 710 nm to 520 nm, corresponding to an aspect ratio change from 2.8 to 1. TEM confirmed that the volume of the AuNR was conserved and the crystalline structure was maintained (Figure 5, SI16). Similar to thermally activated redox processes via thermal anneals,

the extent of reshaping also depends on the composition of, and environment around, the nanocomposite, confirming the importance of local redox chemistry. For example, the reshaping rate is maximum around CTAB:Au concentration ratio above 2 (Figure 5b and c). Again, when the polyol matrix (PVA) and CTAB are entirely replaced it is seen that isovolumetric reshaping will not occur (see SI17).

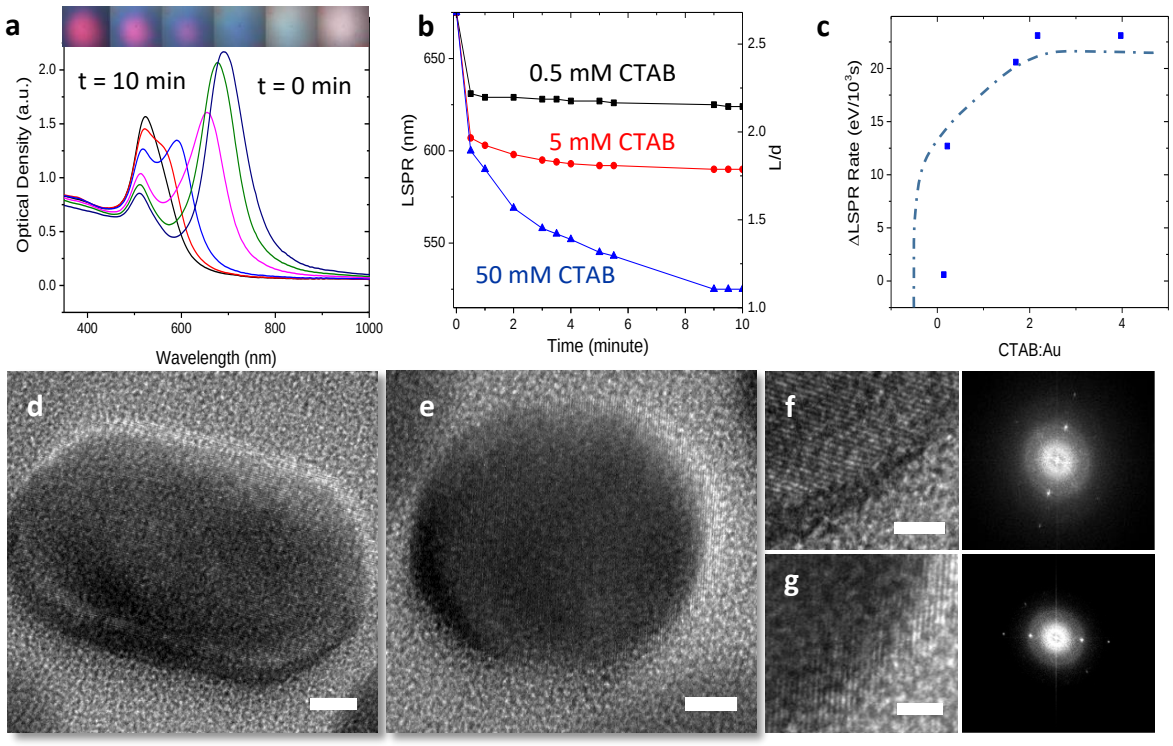

Figure 5. Photo-chemical reshaping of AuNR-PVA films using broadband light. a) Optical micrographs and UV-Vis spectra (taken every ca. 100 seconds) showing reshaping of a nanocomposite (L/d = 2.8, 100 μm thick, ca. 100 nM AuNR, CTAB:Au ratio > 2) over the course of 10 minutes when irradiated with 10 W/cm^2 broadband light (Xe arc lamp) illustrating macroscopic color changes and peak absorption evolution as a function of time. b) The shift in the nanocomposite L-LSPR as a function of time at different CTAB concentrations (L/d = 2.8, 100 μm thick, 50 nM AuNR) when irradiated with 350 long pass broadband light (ca. 10 W/cm^2.) c) The relationship between CTAB:Au as a function of LSPR shift, with peak values in excess of 2 CTAB:Au, similar to that seen using conventional heating processes. d), e) TEM micrographs of

AuNRs at time 0 min and 7 minute, respectively. f), g) HRTEM and FFT demonstrating retention o f crystalline structure at time 0 minute and 7 minute, respectively.

In contrast to redox processes via thermal anneals however, the reshaping rate using light is approximately 2 order of magnitudes faster! Figure 6 compares the rate of reshaping for light with the thermal process in an oven. Overall the light induced process has a slightly larger activation energy than the thermal process (0.86 eV vs 0.65 eV). Also it exhibits a change in reaction order with photo-thermal temperature. The rate is temperature independent at T > 140^{o}C, implying a zeroth order reaction that is only dependent on concentration of reactants. Additionally, the rate is dependent on the optical spectrum, decreasing by a factor of ca. 10 when a long pass filter is used to remove UV (λ_{pass} > 350 nm). However the activation energy and trends are the same (see SI18), indicating that underlying limiting mechanism is the same, and that the relative concentration of reactants is strongly impacted by light.

The Br_2/O_2 - Au oxidation and PVA-Au salt reduction processes are both known to be photo-sensitive. The formation of Br_2 and Br_3^- is accelerated by high pressure Hg or Xe lamp irradiation, exhibiting sensitivity to the visible spectrum. [65,66] For example, CTAB stabilized AuNRs in aqueous solution is observed here to oxidize under irradiation of Xe Light at temperatures as low as 45 ^{o}C in 60 minutes, whereas the same solutions heated to this temperature in an oil bath remain stable (see SI19). The disproportionation and reduction of Au halide salts have also been shown to be accelerated by UV irradiation (e.g. Xe lamp with a band-pass filter for 250-400 nm[39]) (see SI 20). The acceleration of the reaction rate with light is then likely associated with an increase in reactant concentration due to photo-sensitivity of both reduction and oxidation processes.

The decrease in rate, but similar activation energy, upon removal of UV implies that Au halide reduction is not the limiting step in photo-driven reshaping; rather it is likely the PVA-Au salt reduction process. The temperature independence of photo-processes when T > 140°C however indicates that reshaping for these conditions is completely dominated by photo-generation of reactants. Finally, the shift in activation energy between light and thermal driven reshaping probably implies that oxidation, rather than reduction is mechanistically limiting in the absence of light.

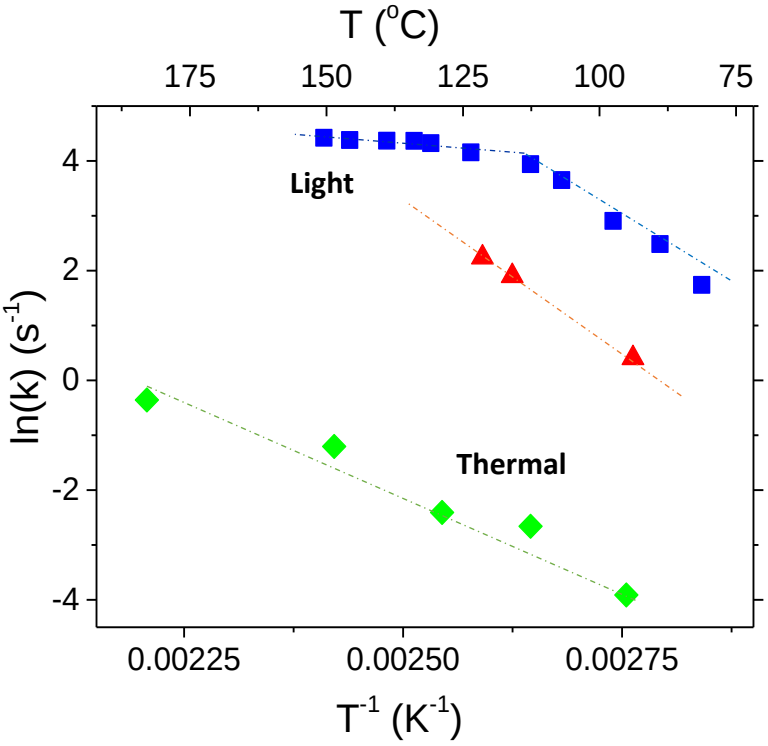

Figure 6. Arrhenius behavior of the reshaping rate for light (red and blue) and thermal (green) processing (typical 100 μm film, 25 mM CTAB, L/d ~2.8, 50 nM AuNR). Light source was an un-polarized broadband light from 1-13 W/cm^2 with (red) and without (blue) a 350 nm long pass filter. The bulk photo-thermal temperature was acquired through FLIR thermal camera.

Optical Patterning

Since reshaping can be achieved within seconds using focused broadband light, and the process controlled via the external environment or film composition, it is possible to realize robust optical patterning with spatial resolution in all three dimensions. For example, Figure 7a-c, demonstrates that a Gaussian intensity profile of a focused spot, results in a Gaussian temperature profile in the film, and a corresponding Gaussian profile of Plasmon resonance. In this case, the lateral gradient of the L-LSPR resonance is 0.01 eV/μm (3 nm/μm). Through thickness optical image reveals an in-plane narrowing with depth of the colored region of reshaped AuNRs consistent with through thickness reduction of optical intensity due to absorption (see SI21). Although not specifically determined, the spatial resolution of the process will likely be limited by the thermal gradient emanating from the central focal point. This could be minimized by active heat removal from the film and enhancing the photochemical sensitivity of the redox process by using bandpass filters.

Overall, the extent of reshaping can be systematically controlled by varying the irradiation power and time. Figure 6d, shows a color map for various combination of exposure time and irradiation power for AuNR-PVA film (AR ~2.8, ca. 50 nM, 25 mM CTAB, 100 μm) without a glass substrate to maximize film heating and reshaping rate. With this data, multicolor images can be inscribed from bitmap files using a single (Figure 7e) or multiple exposure path (Figure 7f).

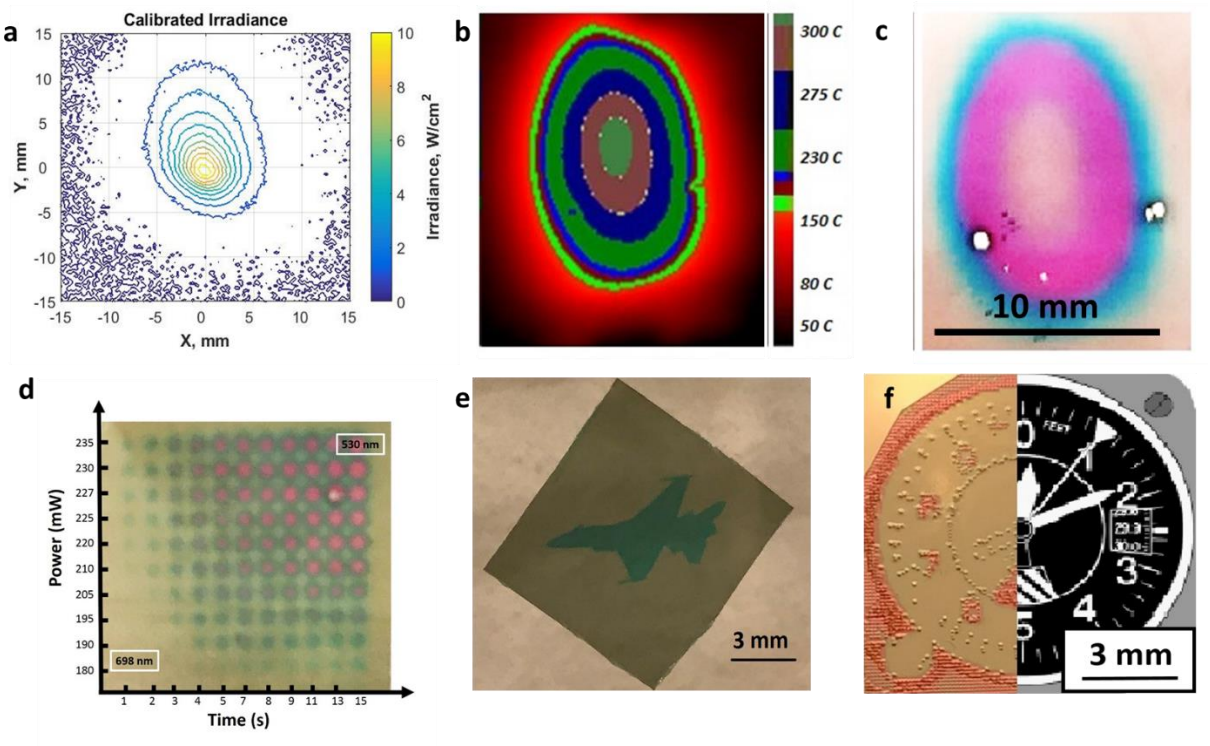

Figure 7. Optical patterning of AuNR-PVA plasmonic nanocomposite. a) Beam profile of a Xenon Arc lamp showing spatial distribution of the irradiation power density. b) Corresponding temperature profile induced from irradiating a AuNR-PVA film (AR ~2.8, ca. 50 nM, 25 mM CTAB, 100 μm.) c) Resulting film showing the color gradient. d) Color map for various combination of exposure time and irradiation power for AuNR-PVA film (AR ~2.8, ca. 50 nM, 25 mM CTAB, 100 μm) without a glass substrate. Each spot ca. 1.5 mm. e) Example binary pattern formation (ca. 40 mW/cm^2, spot size 100 μm, irradiation time 100 ms.) f) Example of a multi-exposure image of reshaped AuNRs where irradiation time alternates between 750 ms and 1500 ms.

Finally due to the speed and localization of the processes, reshaping can be achieved while retaining AuNR alignment, resulting in patterned absorptive polarizers. Uniaxial alignment of AuNRs can be obtained by mechanical stretching the PVA nanocomposite to align the long axis of the AuNR parallel to the stretch direction, Figure 8a.[7] Figure 8b shows the transmission spectra of such an aligned AuNR-PVA film (draw ratio~4.) Strong L-LSPR (680 nm) and L-TSPR (520 nm) absorption is seen when the incident light is polarized parallel or orthogonal to the stretch

direction, respectively. The dichroic ratio at the L-LSPR is 12 dB, and the Herman's orientation factor of the AuNRs is approximately 0.8. [67] An "X" of reshaped nanorods have been written into the AuNR-PVA film in Figure 8c. Since the T-LSPR is not sensitive to the AuNR aspect ratio, the pattern is not seen when observed by light polarized perpendicular to the stretch direction. In contrast, when illuminated by light polarized parallel to stretching direction the colored pattern appears since the AuNR aspect ratio has been reduced. Figure 8d shows the absorption spectra under linearly polarized light of the reshaped region, demonstrating the retention of the dichroic ratio and thus AuNR alignment. This further confirms the localized nature of the reshaping process; that is reshaping occurs sufficiently fast that thermal randomization of rod alignment does not occur. While the matrix is locally heated to allow for atom migration and surface chemistry, the matrix remains sufficiently rigid such that AuNR rotation will not occur. This contrasts work done by Clarke and coworkers where AuNR rotation and subsequent realignment had been demonstrated. [68,69]

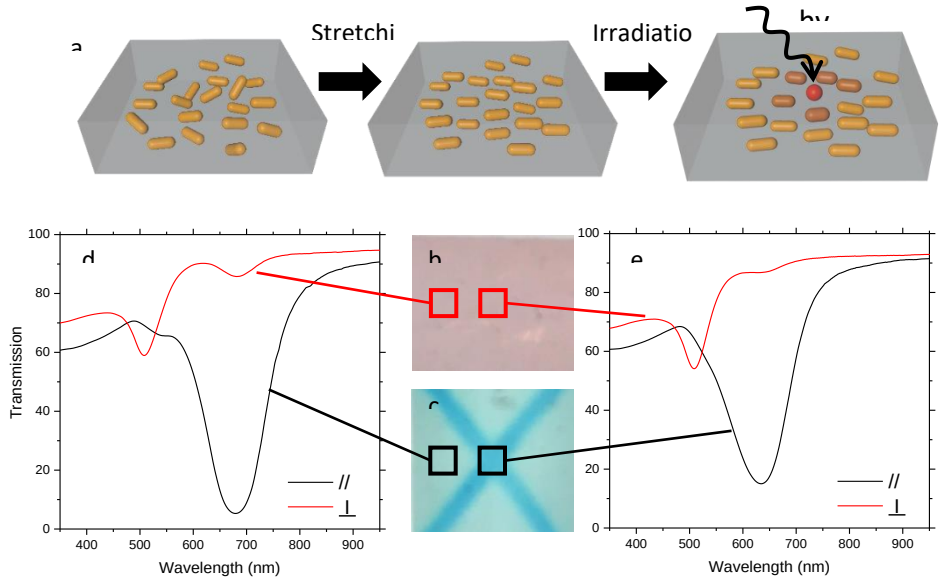

Figure 8. Optical patterning of aligned AuNR-PVA plasmonic nanocomposite. a) Scheme summarizing the process of obtaining alignment of AuNRs and subsequent patterning. b & c) Patterned AuNR-PVA film illuminated by light polarized perpendicular to the stretching direction and by light polarized parallel to the stretching direction, respectively. d & e) Transmission spectra of background area, and patterned area, respectively. Black curve: spectrum from polarization parallel to the stretching direction; red curve: spectrum from polarization perpendicular to stretching direction.

Conclusion

Spatially selective reshaping of AuNRs in PVA has been demonstrated through a chemical redox process. Using broadband visible light to both heat and enhance redox processes, the AuNRs can be isovolumetrically reshaped from AR = 2.8 to AR = 1 as little as 15 seconds. The rate and extent of reshaping can be altered through selectively varying key parameters such as bromide and oxygen content as well as adjusting general components such as temperature, resulting in tuning of the AuNR aspect ratio and thus optical properties. These findings point out that chemistry can also be a contributor to reshaping in solids, that the rate of reshaping need not depend only on

temperature, and in some systems (e.g PVA-AuNR) chemistry can even be the major contributor to reshaping. Relative to reshaping approaches based on "thermal-driven" surface diffusion, incorporation of surface chemistry accelerates reshaping by several orders of magnitude while simultaneously lowering the energy cost (10 W/cm^2 vs 10^{10} W/cm^2). The lower optical power and temperatures preserve the mechanical properties of the matrix. Additional understanding of localized redox processes at the nanoparticle surface will be crucial to expand these concepts to a broader range of nanoparticles and matrices, as well as increasing spatial resolution. Such low energy, optically driven processes are promising routes to cost-effective, rapid manufacture of materials with pixilated, voxelated or gradient plasmonic properties for opto-electronics, colorimetric sensors, polarization sensitive filters, and imaging taggants.

Supporting Information

Supporting information is available free of charge on....[XXXX]. Additional information on solution studies, isovolumetric dimensional analysis, thermal modelling, and activation energy of thermal and photo induced reshaping available in SI.

Acknowledgements

The authors extend their appreciation to Dr. Kenneth Williamson for help with thermal imaging and large scale reshaping. This research was supported by the Air Force Research Laboratory's Materials and Manufacturing Directorate and the Air Force Office of Scientific Research (AFOSR).

CM acknowledges support of the National Research Council Fellowship Program (NRC-RAP). The graphic altimeter was used from wikimedia commons under the public domain.

Methods

Materials: Hexadecyltrimethylammonium bromide (CTAB) was purchased from GFS chemicals. Hexadecyltrimethylammonium chloride (CTAC) was purchased from Aldrich. Benzyldimethylhexadecylammonium chloride (BDAC) was purchased from TCI America. $HAuCl_4$, $AgNO_3$, sodium borohydride and L-ascorbic acid were purchased from Aldrich. Polyvinylalcohol (PVA, M_W = 89,000-98,000, 99+% hydrolyzed, T_g = 80 ºC) and polyethylene oxide (PEO, M_W=35,000, T_g = 65 ºC) were purchased from Sigma-Aldrich. Thiol terminated polystyrene (PS-SH, MW = 10,000) and bulk polystyrene (MW = 35,000) were purchased from Polymer Source and Sigma-Aldrich, respectively.

Synthesis of AuNRs and fabrication of AuNR/polymer composites: The AuNRs were synthesized according to seed growth method modified for scale up production.[11] AuNR dimensions were determined through both UV-Vis spectroscopy as well as TEM image analysis. As-made AuNRs were purified from the growth solution via a series of centrifugation steps to remove unreacted reactants. The initial growth solution was first centrifuged at 8500 RCF (relative centrifugal force) in a 50 mL tube for 30 minutes. The sedimented nanorods were then transferred to a 2 mL centrifuge tube and subsequently spun at 9600 RCF for 30 minutes. After centrifugation, the

supernatant was removed and replaced with a 25 mM CTAB/DI-H_2O solution. This washing step was repeated two times. The solution of AuNRs was then stored (aged) at room temperature and standard pressure in a 20 mL vial for an additional 3 days before film fabrication unless otherwise noted. Note that chemical reactivity of AuNRs is known to depend on aging time and conditions (e.g. temperate, concentration of CTAB, molarity, oxygen exposure, etc.).[70] To avoid this additional variability, experimental series were conducted with the same AuNR batch that had the same preparation and storage conditions. For the PS grafted AuNRs, a ligand exchange was done through solvent transfer processes of CTAB coated AuNRs in DI-H_2O to PS-SH (10 mM) in toluene.[49]

To fabricate films, the AuNR stock solution was added to 2 mL solution of 10 wt % PVA in H_2O (or 10 wt% PS in toluene for the PS-grafted AuNRs.) To vary the amount of CTAB in AuNR films, either additional CTAB was added to the solution before drop casting, or an additional wash step was implemented to remove excess CTAB. The amount of CTAB was confirmed through UV-Vis. The AuNRs - PVA/H_2O (or PS/toluene) solution was homogenously mixed through bath sonication, after which was left to settle, in the case of any potential bubbles that formed in the solution from sonication. After settling, the solution was drop cast on 2 in x 2 in glass slides and spread evenly across the glass for controlled solution casting. After drop casting, the films were left to dry overnight. The concentration of AuNRs was determined using Beer-Lambert's Law where film thickness was measured with a micrometer, optical density was determined at the longitudinal surface plasmon resonance (L-LSPR) peak using UV-Vis-NIR spectroscopy and extinction coefficient for NRs of a given dimension was used from previous literature.[5] Films of

aligned AuNRs were prepared by post-process through incremental stretching of the PVA composite briefly exposed to elevated temperatures at 90 ^{o}C (10 ^{o}C above T_g).

Thermal and photo-thermal processing of AuNRs/polymer nanocomposites: For thermal processing, films were placed in a conventional oven or on a calibrated gradient hot plate. For photo-thermal processing, a CRAIC Xe Arc Lamp was used as a light source (approximated power density ranged from ca. 1-13 W/cm^2, spot size ca. 1.5 mm diameter). Unless otherwise noted, the solid AuNR/PVA films were mounted on a conventional glass slide. The reported optical power densities were experimentally determined using a Thor Labs thermal power meter (model S302C.) The bulk temperature of the photo-thermal processed films was estimated by a calibrated IR camera (Model FLIR SC620).

Solution studies: The solution studies of thermal and photo-thermal reshaping were done in round bottom flasks with 10 mL solution (ca. 1 nM AuNR and 100 mM CTAB / CTAC solution) exposed to either ambient, or argon environments. The solutions were heated to 90 ^{o}C and aliquots at incremental times were taken. The UV-Vis spectra from the aliquots were then subsequently evaluated using Cary 300 Spectrophotometer.

Optical patterning: The color map for various combination of exposure time and irradiation power was produced using broadband light from the CRAIC at varying exposure times and power

densities. The film was not mounted on glass. The printed thunderbird film was acquired using a diode pumped solid state laser at 442 nm wavelength with a spot size of 100 μm, power density of 40 mW/cm^2 and irradiation time of 500 ms. For the altimeter film, similar specifications were used, however two exposure times (750 ms and 1500 ms) were chosen to reshape the rods to AR = 2 and AR = 1, respectively.

Characterization: UV-Vis-NIR spectra of solutions and films were acquired with Cary 300, Cary 5000 UV-Vis-NIR spectrophotometer and CRAIC microspectrometer. Morphology and mean size of nanoparticles were determined by TEM (Philips CM200 LaB6 at 200kV), HR TEM(FEI Cs-corrected Titan at 300 kV), and STEM (FEI Talos at 200 kV). To characterize the reshaped AuNRs, The AuNRs were extracted by dissolving the PVA films in water. UV-Vis spectra were taken to determine the optical change. The centrifugation was employd to purify and concentrate the AuNRs which were subsequently drop casted onto a carbon supported TEM grid. For each sample, more than 500 particles were measured to obtain the average size and the size distribution through Image J analysis.

Reference

(1) Chen, H.; Shao, L.; Li, Q.; Wang, J.: Gold nanorods and their plasmonic properties. *Chem Soc Rev* **2013**, *42*, 2679-724.

(2) Mayer, K. M.; Hafner, J. H.: Localized Surface Plasmon Resonance Sensors. *Chemical Reviews* **2011**, *111*, 3828-3857.

(3) Biswas, S.; Nepal, D.; Park, K.; Vaia, R. A.: Orientation sensing with color using plasmonic gold nanorods and assemblies. *The Journal of Physical Chemistry Letters* **2012**, *3*, 2568-2574.

(4) Biswas, S.; Duan, J.; Nepal, D.; Pachter, R.; Vaia, R.: Plasmonic Resonances in Self-Assembled Reduced Symmetry Gold Nanorod Structures. *Nano Letters* **2013**, *13*, 2220-2225.

(5) Park, K.; Biswas, S.; Kanel, S.; Nepal, D.; Vaia, R. A.: Engineering the Optical Properties of Gold Nanorods: Independent Tuning of Surface Plasmon Energy, Extinction Coefficient, and Scattering Cross Section. *The Journal of Physical Chemistry C* **2014**, *118*, 5918-5926.

(6) Biswas, S.; Liu, X.; Jarrett, J. W.; Brown, D.; Pustovit, V.; Urbas, A.; Knappenberger, K. L.; Nealey, P. F.; Vaia, R. A.: Nonlinear Chiro-Optical Amplification by Plasmonic Nanolens Arrays Formed via Directed Assembly of Gold Nanoparticles. *Nano Letters* **2015**, *15*, 1836-1842.

(7) Melissa Maldonado, H. B., Anderson SL Gomes, R Vaia, K Park, J Che, M Hsiao, Cid B de Araújo, A Baev, PN Prasad: Coupled-plasmon induced optical nonlinearities in anisotropic arrays of gold nanorod clusters supported in a polymeric film. *Journal of Applied Physics* **2017**, *121*, 143103.

(8) Vigderman, L.; Khanal, B. P.; Zubarev, E. R.: Functional Gold Nanorods: Synthesis, Self-Assembly, and Sensing Applications. *Advanced Materials* **2012**, *24*, 4811-4841.

(9) Zijlstra, P.; Chon, J. W. M.; Gu, M.: Five-dimensional optical recording mediated by surface plasmons in gold nanorods. *Nature* **2009**, *459*, 410-413.

(10) Jain, P. K.; Huang, X.; El-Sayed, I. H.; El-Sayed, M. A.: Review of Some Interesting Surface Plasmon Resonance-enhanced Properties of Noble Metal Nanoparticles and Their Applications to Biosystems. *Plasmonics* **2007**, *2*, 107-118.

(11) Park, K.; Hsiao, M.-s.; Yi, Y.-J.; Izor, S.; Koerner, H.; Jawaid, A.; Vaia, R. A.: Highly Concentrated Seed-Mediated Synthesis of Monodispersed Gold Nanorods. *ACS Applied Materials & Interfaces* **2017**.

(12) Henry, A.-I.; Bingham, J. M.; Ringe, E.; Marks, L. D.; Schatz, G. C.; Van Duyne, R. P.: Correlated Structure and Optical Property Studies of Plasmonic Nanoparticles. *The Journal of Physical Chemistry C* **2011**, *115*, 9291-9305.

(13) Olson, J.; Dominguez-Medina, S.; Hoggard, A.; Wang, L. Y.; Chang, W. S.; Link, S.: Optical characterization of single plasmonic nanoparticles. *Chemical Society Reviews* **2015**, *44*, 40-57.

(14) Liu, Y.; Mills, E. N.; Composto, R. J.: Tuning optical properties of gold nanorods in polymer films through thermal reshaping. *Journal of Materials Chemistry* **2009**, *19*, 2704.

(15) Taylor, A.; Siddiquee, A.; Chon, J.: Below Melting Point Photothermal Reshaping of Single Gold Nanorods Driven by Surface Diffusion. *ACS Nano* **2014**, *8*, 12071–12079.

(16) Zijlstra, P.; Chon, J. W.; Gu, M.: Five-dimensional optical recording mediated by surface plasmons in gold nanorods. *Nature* **2009**, *459*, 410-3.

(17) Pérez-Juste, J.; Rodríguez-González, B.; Mulvaney, P.; Liz-Marzán, L. M.: Optical Control and Patterning of Gold-Nanorod-Poly(vinyl alcohol) Nanocomposite Films. *Advanced Functional Materials* **2005**, *15*, 1065-1071.

(18) Mohamed, M.; Ismail, K.; Link, S.; El-Sayed, M.: Thermal Reshaping of Gold Nanorods in Micelles. *Journal of Physical Chemistry B* **1998**, *102*, 9370-9374.

(19) Plowman, B. J.; Thompson, N.; O'Mullane, A. P.: Probing the surface oxidation of chemically synthesised gold nanospheres and nanorods. *Gold Bulletin* **2014**, *47*, 177-183.

(20) Rodríguez-Lorenzo, L.; Romo-Herrera, J. M.; Pérez-Juste, J.; Alvarez-Puebla, R. A.; Liz-Marzán, L. M.: Reshaping and LSPR tuning of Au nanostars in the presence of CTAB. *Journal of Materials Chemistry* **2011**, *21*, 11544.

(21) Zhu, Q. N.; Wu, J.; Zhao, J. W.; Ni, W. H.: Role of Bromide in Hydrogen Peroxide Oxidation of CTAB-Stabilized Gold Nanorods in Aqueous Solutions. *Langmuir* **2015**, *31*, 4072-4077.

(22) Petrova, H.; Perez Juste, J.; Pastoriza-Santos, I.; Hartland, G. V.; Liz-Marzan, L. M.; Mulvaney, P.: On the temperature stability of gold nanorods: comparison between thermal and ultrafast laser-induced heating. *Phys Chem Chem Phys* **2006**, *8*, 814-21.

(23) Link, S.; Wang, Z.; El-Sayed, M.: How Does a Gold Nanorod Melt? *Journal of Physical Chemistry B* **2000**, *104*.

(24) Zijlstra, P.; Chon, J.; Gu, M.: Effect of heat accumulation on the dynamic range of a gold nanorod doped polymer nanocomposite for optical laser writing and patterning. *Optical Society of America* **2007**, *15*, 12151.

(25) Cong, B.; Kan, C.; Wang, H.; Liu, J.; Xu, H.; Ke, S.: Gold Nanorods: Near-Infrared Plasmonic Photothermal Conversion and Surface Coating. *Journal of Materials Science and Chemical Engineering* **2014**, *02*, 20-25.

(26) Nepal, D.; Park, K.; Vaia, R. A.: High-Yield Assembly of Soluble and Stable Gold Nanorod Pairs for High-Temperature Plasmonics. *Small* **2012**, *8*, 1013-1020.

(27) Li, Y.; Jiang, Z.; Lin, X. M.; Wen, H.; Walko, D. A.; Deshmukh, S. A.; Subbaraman, R.; Sankaranarayanan, S. K.; Gray, S. K.; Ho, P.: Femtosecond laser pulse driven melting in gold nanorod aqueous colloidal suspension: identification of a transition from stretched to exponential kinetics. *Sci Rep* **2015**, *5*, 8146.

(28) Taylor, A. B.; Chow, T. T. Y.; Chon, J. W. M.: Alignment of gold nanorods by angular photothermal depletion. *Applied Physics Letters* **2014**, *104*, 083118.

(29) Link, S.; Burda, C.; Mohamed, M.; Nikoobakht, B.; El-Sayed, M.: Laser Photothermal Melting and Fragmentation of Gold Nanorods: Energy and Laser Pulse-Width Dependence. *Journal of Physical Chemistry A* **1999**, *103*.

(30) Maity, S.; Bochinski, J. R.; Clarke, L. I.: Metal Nanoparticles Acting as Light-Activated Heating Elements within Composite Materials. *Advanced Functional Materials* **2012**, *22*, 5259-5270.

(31) Chon, J. W. M.; Bullen, C.; Zijlstra, P.; Gu, M.: Spectral encoding on Gold Nanorods Doped in a Silica Sol–Gel Matrix and Its Application to High-Density Optical Data Storage. *Advanced Functional Materials* **2007**, *17*, 875-880.

(32) Gonzalez-Rubio, G.; Guerrero-Martinez, A.; Liz-Marzan, L. M.: Reshaping, Fragmentation, and Assembly of Gold Nanoparticles Assisted by Pulse Lasers. *Acc Chem Res* **2016**, *49*, 678-86.

(33) Zijlstra, P.; Chon, J. W. M.; Gu, M.: White light scattering spectroscopy and electron microscopy of laser induced melting in single gold nanorods. *Physical Chemistry Chemical Physics* **2009**, *11*, 5915-5921.

(34) Marie Paule, P.: Nano-supracrystallinity. *EPL (Europhysics Letters)* **2015**, *109*, 58001.

(35) Qin, Z. P.; Wang, Y. R.; Randrianalisoa, J.; Raeesi, V.; Chan, W. C. W.; Lipinski, W.; Bischof, J. C.: Quantitative Comparison of Photothermal Heat Generation between Gold Nanospheres and Nanorods. *Scientific Reports* **2016**, *6*.

(36) Lee, J. H.; Gibson, K. J.; Chen, G.; Weizmann, Y.: Bipyramid-templated synthesis of monodisperse anisotropic gold nanocrystals. *Nat Commun* **2015**, *6*, 7571.

(37) Attia, Y. A.; Buceta, D.; Requejo, F. G.; Giovanetti, L. J.; Lopez-Quintela, M. A.: Photostability of gold nanoparticles with different shapes: the role of Ag clusters. *Nanoscale* **2015**, *7*, 11273-11279.

(38) Long, R.; Zhou, S.; Wiley, B. J.; Xiong, Y.: Oxidative etching for controlled synthesis of metal nanocrystals: atomic addition and subtraction. *Chem Soc Rev* **2014**, *43*, 6288-310.

(39) Eustis, S.; Hsu, H.-Y.; El-Sayed, M. A.: Gold Nanoparticle Formation from Photochemical Reduction of Au3+ by Continuous Excitation in Colloidal Solutions. A Proposed Molecular Mechanism. *The Journal of Physical Chemistry B* **2005**, *109*, 4811-4815.

(40) Deng, T. S.; van der Hoeven, J. E. S.; Yalcin, A. O.; Zandbergen, H. W.; van Huis, M. A.; van Blaaderen, A.: Oxidative Etching and Metal Overgrowth of Gold Nanorods within Mesoporous Silica Shells. *Chemistry of Materials* **2015**, *27*, 7196-7203.

(41) Tsung, C. K.; Kou, X. S.; Shi, Q. H.; Zhang, J. P.; Yeung, M. H.; Wang, J. F.; Stucky, G. D.: Selective shortening of single-crystalline gold nanorods by mild oxidation. *Journal of the American Chemical Society* **2006**, *128*, 5352-5353.

(42) Jang, E.; Lim, E.-K.; Choi, J.; Park, J.; Huh, Y.-J.; Suh, J.-S.; Huh, Y.-M.; Haam, S.: Br-Assisted Ostwald Ripening of Au Nanoparticles under H2O2 Redox. *Crystal Growth & Design* **2012**, *12*, 37-39.

(43) Guirguis, O. W.; Moselhey, M. T. H.: Thermal and structural studies of poly (vinyl alcohol) and hydroxypropyl cellulose blends. *Natural Science* **2012**, *04*, 57-67.

(44) Strawhecker, K.; Manias, E.: Structure and Properties of Poly(vinyl alcohol)/Na+ Montmorillonite Nanocomposites. *Chem. Mater.* **2000**, *12*, 2943-2949.

(45) Holland, B. J.; Hay, J.: *The thermal degradation of poly(vinyl alcohol)*, 2001; Vol. 42.

(46) Thomas, P. S.; Guerbois, J.-P.; Russell, G. F.; Briscoe, B. J.: FTIR Study of the Thermal Degradation of Poly(vinyl Alcohol). *Journal of Thermal Analysis and Calorimetry* **2001**, *64*, 501-508.

(47) Taylor, A. B.; Siddiquee, A. M.; Chon, J. W. M.: Below Melting Point Photothermal Reshaping of Single Gold Nanorods Driven by Surface Diffusion. *ACS Nano* **2014**, *8*, 12071-12079.

(48) Rostro-Kohanloo, B. C.; Bickford, L. R.; Payne, C. M.; Day, E. S.; Anderson, L. J. E.; Zhong, M.; Lee, S.; Mayer, K. M.; Zal, T.; Adam, L.; Dinney, C. P. N.; Drezek, R. A.; West, J. L.; Hafner, J. H.: The stabilization and targeting of surfactant-synthesized gold nanorods. *Nanotechnology* **2009**, *20*.

(49) Park, K.; Drummy, L. F.; Wadams, R. C.; Koerner, H.; Nepal, D.; Fabris, L.; Vaia, R. A.: Growth mechanism of gold nanorods. *Chemistry of Materials* **2013**, *25*, 555-563.

(50) Yuan, H.; Janssen, K. P. F.; Franklin, T.; Lu, G.; Su, L.; Gu, X.; Uji-i, H.; Roeffaers, M. B. J.; Hofkens, J.: Reshaping anisotropic gold nanoparticles through oxidative etching: the role of the surfactant and nanoparticle surface curvature. *RSC Advances* **2015**, *5*, 6829-6833.

(51) Rao, V. K.; Radhakrishnan, T. P.: Tuning the SERS Response with Ag-Au Nanoparticle-Embedded Polymer Thin Film Substrates. *Acs Applied Materials & Interfaces* **2015**, *7*, 12767-12773.

(52) Porel, S.; Singh, S.; Harsha, S. S.; Rao, D. N.; Radhakrishnan, T. P.: Nanoparticle-embedded polymer: In situ synthesis, free-standing films with highly monodisperse silver nanoparticles and optical limiting. *Chemistry of Materials* **2005**, *17*, 9-12.

(53) Dong, H.; Chen, Y. C.; Feldmann, C.: Polyol synthesis of nanoparticles: status and options regarding metals, oxides, chalcogenides, and non-metal elements. *Green Chemistry* **2015**, *17*, 4107-4132.

(54) Longenberger, L.; Mills, G.: FORMATION OF METAL PARTICLES IN AQUEOUS-SOLUTIONS BY REACTIONS OF METAL-COMPLEXES WITH POLYMERS. *Journal of Physical Chemistry* **1995**, *99*, 475-478.

(55) Ni, W.; Kou, X.; Yang, Z.; Wang, J. F.: Tailoring longitudinal surface plasmon wavelengths, scattering and absorption cross sections of gold nanorods. *Acs Nano* **2008**, *2*, 677-686.

(56) Gou, L.; Murphy, C. J.: Fine-Tuning the Shape of Gold Nanorods. *Chemistry of Materials* **2005**, *17*, 3668-3672.

(57) Ni, W. H.; Ba, H. J.; Lutich, A. A.; Jackel, F.; Feldmann, J.: Enhancing Single-Nanoparticle Surface-Chemistry by Plasmonic Overheating in an Optical Trap. *Nano Letters* **2012**, *12*, 4647-4650.

(58) Lamarche, F.; Leroy, C.: Evaluation of the volume of intersection of a sphere with a cylinder by elliptic integrals. *Computer Physics Communications* **1990**, *59*, 359-369.

(59) Baffou, G.; Quidant, R.; Girard, C.: Heat generation in plasmonic nanostructures: Influence of morphology. *Applied Physics Letters* **2009**, *94*, 153109.

(60) Viswanath, V.; Maity, S.; Bochinski, J. R.; Clarke, L. I.; Gorga, R. E.: Thermal Annealing of Polymer Nanocomposites via Photothermal Heating: Effects on Crystallinity and Spherulite Morphology. *Macromolecules* **2013**, *46*, 8596-8607.

(61) Bergman, T.; Lavine, A.; Incropera, F.; D., D.: *Fundamentals of Heat and Mass Transfer*; 7th ed.; Wiley, 2011.

(62) Losego, M. D.; Grady, M. E.; Sottos, N. R.; Cahill, D. G.; Braun, P. V.: Effects of chemical bonding on heat transport across interfaces. *Nat Mater* **2012**, *11*, 502-6.

(63) Ekici, O.; Harrison, R. K.; Durr, N. J.; Eversole, D. S.; Lee, M.; Ben-Yakar, A.: Thermal Analysis of Gold Nanorods Heated with Femtosecond Laser Pulses. *J Phys D Appl Phys* **2008**, *41*, 185501.

(64) Amjad, M.; Raza, G.; Xin, Y.; Pervaiz, S.; Xu, J.; Du, X.; Wen, D.: Volumetric solar heating and steam generation via gold nanofluids. *Applied Energy* **2017**, *206*, 393-400.

(65) Dabestani, R.; Wang, X.; Bard, A. J.; Campion, A.; Fox, M. A.; Webber, S. E.; White, J. M.: Photoinduced oxidation of bromide to bromine on irradiated platinized titanium dioxide powders and platinized titanium dioxide particles supported on Nafion films. *The Journal of Physical Chemistry* **1986**, *90*, 2729-2732.

(66) Halmann, M.; Porat, Z.: Photooxidation of bromide to bromine in dead sea water. *Solar Energy* **1988**, *41*, 417-421.

(67) Sinha-Ray, S.; Fezzaa, K.; Yarin, A. L.: The internal structure of suspensions in uniaxial elongation. *Journal of Applied Physics* **2013**, *113*.

(68) Maity, S.; Wu, W. C.; Tracy, J. B.; Clarke, L. I.; Bochinski, J. R.: Nanoscale steady-state temperature gradients within polymer nanocomposites undergoing continuous-wave photothermal heating from gold nanorods. *Nanoscale* **2017**, *9*, 11605-11618.

(69) Maity, S.; Wu, W. C.; Xu, C.; Tracy, J. B.; Gundogdu, K.; Bochinski, J. R.; Clarke, L. I.: Spatial temperature mapping within polymer nanocomposites undergoing ultrafast photothermal heating via gold nanorods. *Nanoscale* **2014**, *6*, 15236-47.

(70) Tong, W.; Katz-Boon, H.; Walsh, M. J.; Weyland, M.; Etheridge, J.; Funston, A. M.: The evolution of size, shape, and surface morphology of gold nanorods. *Chemical Communications* **2018**, 54, 3022-3025/

Table of Content Figure

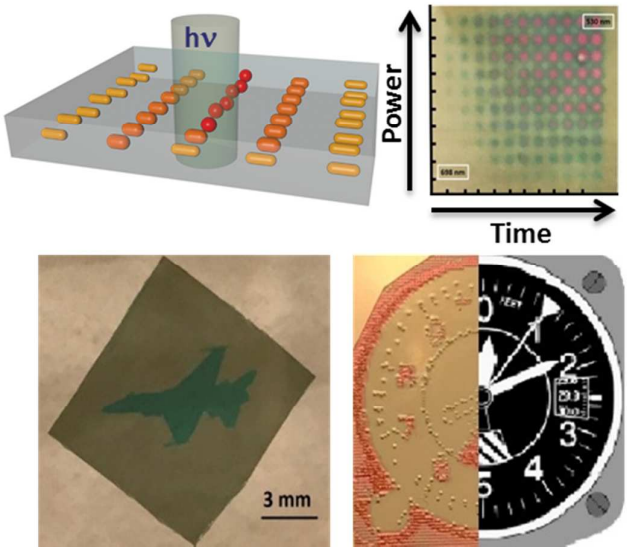

Light-triggered reduction and oxidation processes enable isovolumetric reshaping of AuNRs in a polymer matrix and printing of complex patterns with multiple plasmonic characteristics.